Directionality in the GammaTracker Handheld Radioisotope Identifier

Carolyn E. Seifert, *Member, IEEE*, Mitchell J. Myjak, *Member, IEEE*

***Abstract*—Several computationally simple methods are presented for determining the direction to one or more radiation sources using the GammaTracker handheld radioisotope identifier. GammaTracker will display a heading indicating the direction to one or more sources; no gamma-ray images will be shown to the user. The details of each directionality method are presented and performance is compared using radiation transport simulations of gamma-ray point sources at varying activity levels on a natural background. All methods achieved sufficiently high pointing accuracy and precision in the tested scenarios, which included background-to-source ratios up to 10:1. The prospects for implementation in the GammaTracker firmware architecture are discussed.**

***Index Terms*— Gamma-ray spectroscopy detectors, nuclear imaging, directional detectors, pixel detectors**

I. Introduction

THE GammaTracker handheld radioisotope identifier is a high-efficiency, high-resolution spectrometer for real-time search, survey and characterization. The system incorporates eighteen 1.5 cm × 1.5 cm × 1.0 cm Cd-Zn-Te detectors capable of 1% FWHM energy resolution at 662 keV; through pixellation the detectors have a discretized position resolution of approximately 1.2 mm × 1.2 mm × 0.5 mm. The detectors are arranged in two 3 × 3 arrays for a relative detection efficiency of 20% [1]. The GammaTracker system design is presented in [2], and only a brief discussion of the imaging components is presented here.

For each gamma-ray interaction in the Cd-Zn-Te array, the 3-D position and energy are measured in the same manner as the University of Michigan Polaris system [3]. Measurements from gamma rays that interact more than once in the array are passed to the "two-cone" Compton backprojection algorithm (also called the "method of intersections"), which generates a list of intersection points between pairs of Compton cones on the unit sphere. As described in [4], this reconstruction method eliminates the need to trace individual cones onto the sphere, is computationally simpler than traditional backprojection methods for reasonable numbers of cones, and improves the ability to detect weak sources if one only intersects pairs of cones with similar energies. In addition, the method is easily implemented on the embedded FPGA used in the GammaTracker instrument for data acquisition and processing. The system uses the results of the two-cone algorithm to calculate a horizontal direction to the source or sources. To expedite source search, only the direction is displayed on the screen.

Simple methods that take advantage of low-count statistics for calculating directionality are preferred for this handheld instrument, not only to ensure accurate operation in low radiation fields, but also to allow the directionality computations to be performed on the embedded FPGA. This Xilinx Spartan-3 FPGA clearly has limited computational resources compared to a desktop computer, and is also only clocked at 50 MHz to save power.

Compton backprojection is a well-known technique for imaging radiation sources, but much of the research emphasis has been on obtaining high-resolution images, not directionality. One direction-finding algorithm proposed by Lackie et al. simplifies the imaging calculations by intersecting the bounding rectangles for each circular projection [5]. As the intersection of two rectangles is merely another rectangle, the algorithm can progressively refine the current estimate. However, the method currently assumes that only one source is present, and that the number of spurious cones is insignificant. These assumptions become invalid for weak radiation sources with high background rates.

Directionality algorithms that do not use Compton backprojection are also becoming more common. Kaye et al. proposed a method using the physical centroid of observed events to calculate the direction to a source [6]. These algorithms are better suited to finding low-energy gamma-ray sources, such that the attenuation lengths of the gamma rays are short compared to the dimensions of the detector.

In this work, several Compton-based directionality methods are evaluated for incorporation into the GammaTracker instrument. These algorithms are described in Section II. Each method is tested using GEANT4 [7] radiation transport simulations of gamma-ray point sources and realistic soil backgrounds, as presented in Section III. Section IV concludes this work with the potential implementation

Manuscript received June 30, 2008. This work was performed by Pacific Northwest National Laboratory (PNNL) for the National Nuclear Security Administration Office of Nonproliferation Research and Development. PNNL is operated by Battelle Memorial Institute for the U.S. Department of Energy under Contract DE-AC05-76RL01830.

C. E. Seifert is with Pacific Northwest National Laboratory, Richland, WA 99352 USA (phone: 509-376-3915; fax: 509-372-0672; e-mail: carolyn.seifert@pnl.gov).

M. J. Myjak is with Pacific Northwest National Laboratory, Richland, WA 99352 USA. (e-mail: mitchell.myjak@pnl.gov).

.

architectures and relevance of each method for the GammaTracker instrument.

For clarity, in this work we define an event as any detectable gamma-ray interaction in the material. A sequence is series of events observed in the detector from the same gamma ray. Also, we define the energy of a Compton cone as the total energy deposited in the gamma-ray sequence used to reconstruct the cone.

II. Directionality Methods

With sufficient statistics and only a single gamma-ray source, finding the source direction is trivial. The instrument could use the output of the Compton backprojection algorithm to create a 4π spherical image of source density. The pixel with the highest number of counts in the image would indicate the direction to the source; the error in this direction is defined by the image pixel resolution for reasonable pixel sizes. However, this method cannot be used to determine the absence of a source, and it fails for gamma-ray sources in a complex environmental background or for radiation fields involving more than one point source. It is necessary, therefore, to process the gamma-ray imaging data appropriately to determine whether and how many sources are within the instrument field of view.

A. 1-D Summation Projection

One method for determining the direction to the source is to simply collapse the 4π spherical image into a one-dimensional vector representing the heading, by summing the image data along the vertical dimension. Let $M_{\theta\phi}$ be a 4π spherical image with horizontal coordinate θ and vertical coordinate ϕ. The heading vector **d** is given by

$$d_\theta = \sum_{\phi=-90^\circ}^{90^\circ} M_{\theta\phi} \ . \qquad (1)$$

The source positions are then determined by finding peaks in the heading vector using traditional peak-pickoff methods.

Notice that the instrument would not have to create $M_{\theta\phi}$, but could increment d_θ for every intersection point. Thus, the complexity of the summation algorithm is $\underline{O}(n + r)$, where n is the number of intersection points, and r the resolution (i.e. the number of angular bins) of vector **d**. (This notation means that the complexity scales linearly with respect to n or r, whichever dominates.)

B. 1-D Maximization Projection

Another straightforward method is to collapse the 4π spherical image into a one-dimensional vector, as in the above method, except that the maximum intensity pixel, rather than the sum of pixels, is taken along the appropriate image index, as given by

$$d_\theta = \max_\phi \{M_{\theta\phi}\}. \qquad (2)$$

Again, traditional peak determination methods are used to find the source locations. Compared to the first approach, the maximization algorithm eliminates the effects of tail-summing on the heading vectors and can improve the ability to distinguish closely spaced sources. However, the complexity scales as $O(n + r^2)$, since the instrument would need to construct the image $M_{\theta\phi}$.

C. Statistically Significant Pixels

The third method involves determining a statistically significant elevation in pixel intensity. A histogram of pixel intensities is generated to determine the average background pixel value. The pixels associated with the source are clearly separated from the image background. Applying an intensity threshold based on the mean pixel intensity (e.g. a 3-sigma threshold) to this data yields a series of pixel groups on the image sphere associated with source positions. Continuity tests are used to determine whether all pixels belong to one source or whether there are multiple sources. Furthermore, completely discontinuous high-intensity pixels are discarded as anomalous because the imaging resolution is known to be several pixels wide, and any real point source will have a number of neighboring pixels with values above the given threshold.

The primary disadvantage of this method is that it may not find a weak source in the presence of stronger sources because the hotspots in the image will result in a significant elevation in the average pixel intensity. The complexity of the statistical algorithm is $O(n + r^2)$.

D. Intersection Clustering

The clustering algorithm works directly with the list of intersection points produced by the "two-cone" Compton backprojection algorithm. Each point specifies the mutual intersection of the unit sphere with two Compton cones of similar energy. For each intersection point i, the algorithm calculates a metric c_i, defined as the number of intersection points within an angular radius of 15° that have an energy difference of 2% or less. The intersection point having the maximum value of c_i is assumed to indicate the direction to the first point source. All intersection points in this "cluster" are removed from the original list, as well as all other intersection points that involve the same pairs of Compton cones. The process is then repeated for the next identified cluster until a maximum number of sources is identified or no additional clusters remain.

The complexity of the clustering algorithm is $O(n^2)$, which becomes more time-consuming for large numbers of intersection points. However, calculating the statistic c_i is computationally simple: taking the dot product between two intersection points produces the cosine of the angular distance between them. In addition, the algorithm does not have to iterate through a 4π spherical image.

E. Intersection Density

The final method performs a similar set of calculations as

the clustering algorithm, except that an intersection density metric ρ_i is calculated between each intersection point *i* and each Compton cone *j*. This metric is defined by

$$\rho_i = \sum_{j=1}^{m} \max\left\{10° - \Delta\alpha_{ij}, 0\right\}, \quad (3)$$

where $\Delta\alpha_{ij}$ is the minimum angular distance between the intersection point *i* and the cone *j*. This metric is calculated only for cones of similar energies and reflects both the number of cones that pass near the vicinity of intersection point *i* and the relative nearness of those cones. The intersection point with the maximum value of ρ_i is assumed to indicate the direction to the first point source. All associated Compton cones and their intersection points are removed from the list, and the process is repeated until no sources are identified or a maximum number of sources have been located.

The complexity of this algorithm is O(*m*•*n*), where *m* is the number of cones and *n* is the number of intersection points. Typically *m* is lower than *n*, so the density algorithm is more efficient than the clustering algorithm in the upper bound. Computing the minimum angular distance between an intersection point and a Compton cone is slightly more complex, but the trigonometry is straightforward.

III. Simulations and Results

A. Method

To evaluate the various directionality algorithms, radiation transport simulations were performed using GEANT4.6.1 with low-energy physics (including Doppler broadening). The exact deposited energies and locations of all gamma-ray interactions in the detector array were recorded. These quantities were then randomly blurred to reflect the actual energy and position resolutions observed in the GammaTracker instrument. Separate radiation transport simulations were performed for point sources in various locations around the detector array, and a representative uniform soil background simulation was also performed. The soil model was generated assuming a density of 1.82 g/cm^3 and primary constituents of O, Si, Ca, Al, Fe, and Mg, with the following radioisotope constituents: 2.44 mg ^{40}K, 9.6 mg ^{232}Th, 19.4 μg ^{235}U, 2.68 mg ^{238}U, and 200 pCi ^{137}Cs (fallout) per kilogram of soil with 10^9 years of grow-in.

To generate image/directionality data, we selected a series of 1000 detected sequences for a given source location using a specified ratio of source and background sequences randomly selected from the generated event files, and these sequences were used to generate a list of Compton cone intersection points with associated gamma-ray energies as in [4]. At expected levels of gamma-ray exposure, directionality must be calculated based on as few sequences as possible. Statistical variations between observed event histories will cause the performance of each method to vary on an image-by-image basis. To overcome any bias introduced by using a limited set of gamma-ray sequences, 100 such realizations of 1000 sequences were separately selected and reconstructed. For the methods that use image data, a 64×32-pixel 4π image was generated from each of the 100 data sets (resulting in an image pixel size of 5.5˚). The directionality algorithms were then applied to either the images or the intersection data directly, as appropriate.

Each method was applied to the same sets of detected sequences, and the calculated source direction was determined for each of the 100 realizations. The accuracy and precision of each method were then evaluated and compared with the other methods.

B. Directionality Performance

A simulated ^{137}Cs source was placed at (+22.5˚, +22.5˚) relative to the modeled GammaTracker instrument as described in Section III A. The data were not filtered for specific energies or minimum separation distance between gamma-ray events. All kinematically possible sequences of two or three events were used to generate the directionality data.

To demonstrate performance of the various algorithms in a low-background environment, the soil background is modeled has having twice the detected intensity as the source. Given the expected background count rate of 8.8 sequences per second [4], a detected source rate of 4.4 sequences per second is equivalent to a 2-μCi ^{137}Cs source located 5 m from the detector. Fig. 1 shows the distribution of calculated directions for each of the five methods for the low-background case. Each of the methods determined the correct direction to within one or two image pixels for all 100 realizations of the source and background in this case.

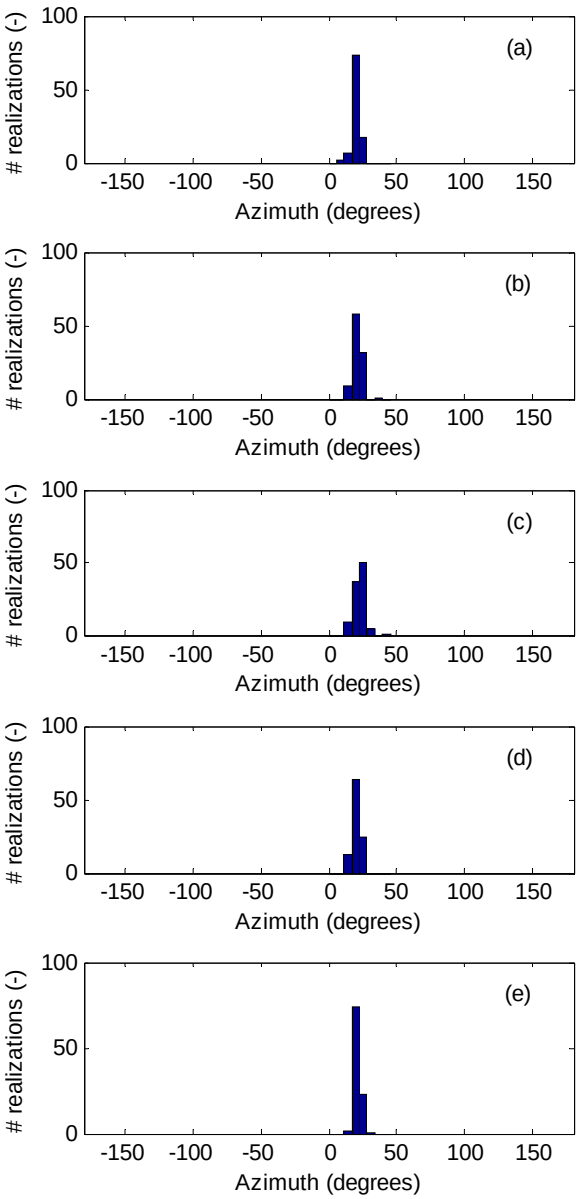

Fig. 1. Distribution of identified source directions for a single ^{137}Cs source on a soil background (2:1 background-to-source ratio) located at 22.5˚ for the (a) summation, (b) maximization, (c) statistical, (d) clustering, and (e) density methods. Image pixel size is 5.5˚.

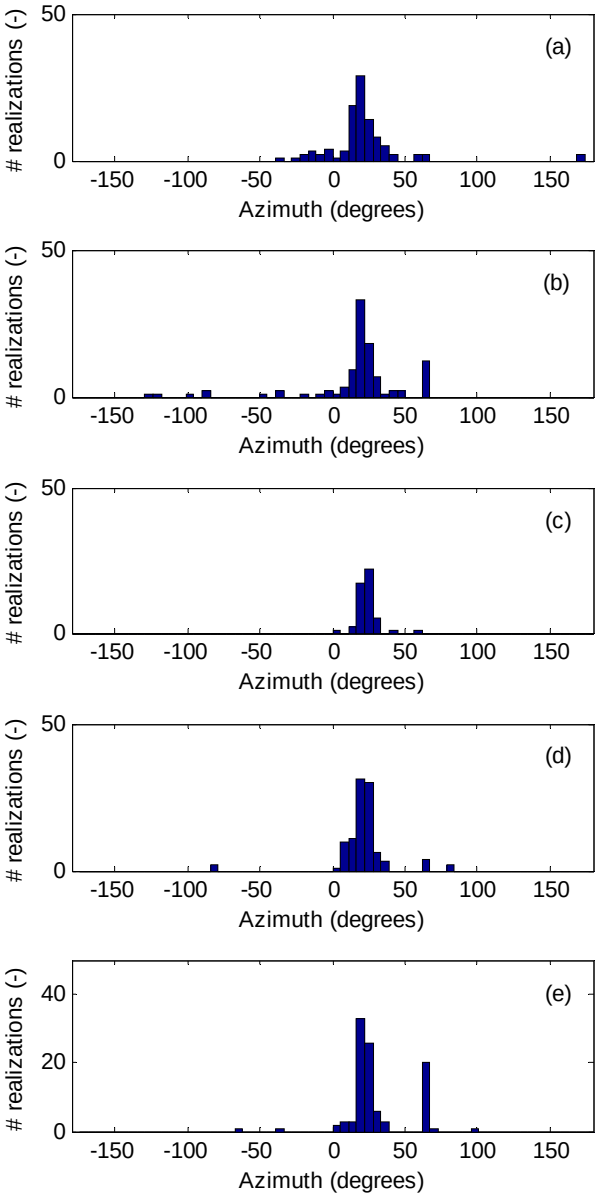

Fig. 2. Distribution of identified source directions for a single ^{137}Cs source on a soil background (10:1 background-to-source ratio) located at 22.5˚ for the (a) summation, (b) maximization, (c) statistical, (d) clustering, and (e) density methods. Image pixel size is 5.5˚.

Then, the background-to-source detected sequence ratio was increased from 2:1 to 10:1, equivalent to placing the 2 μCi source at 11 m. The resulting directional distributions are shown in Fig. 2. Both the summation and maximization methods result in long tails, where many images were incorrectly analyzed. The statistically significant pixel method was more accurate, but also did not find a source at all in many of the images. Both the intersection cluster and density methods identified the majority of source directions correctly, although the latter showed a number of determinations at 65˚.

Finally, two sources were placed 45˚ degrees apart (one at +45˚ and one at +90˚) in the simulation. The ratio of background-to-source detected sequences was kept constant at 10:1 for each source, resulting in an equal number of detected sequences for each source. However, because of the

anisotropy of the GammaTracker instrument (especially

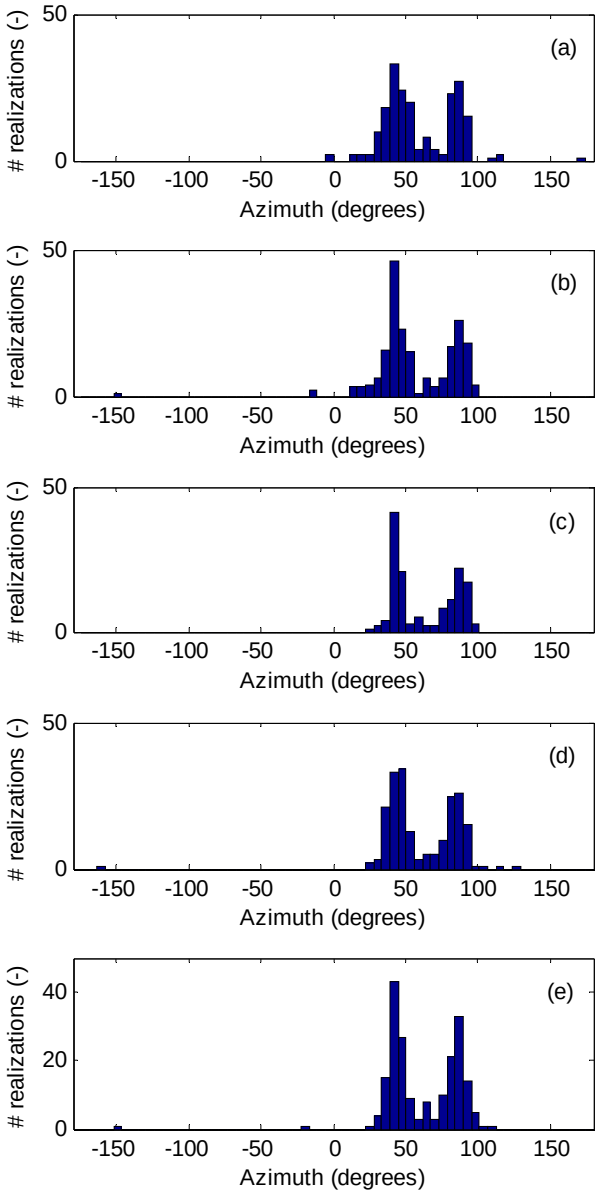

Fig. 3. Distribution of identified source directions for two ^{137}Cs sources on a soil background (10:1 background-to-source ratio) located at 45˚ and 90˚ for the (a) summation, (b) maximization, (c) statistical, (d) clustering, and (e) density methods. Image pixel size is 5.5˚.

at 90˚ where the incoming gamma-ray direction is nearly parallel to the plane of the detector arrays) the number of detected two- and three-event sequences was different for each source, which affects the actual number of imaged sequences.

The resulting distributions for the two-source case are shown in Fig. 3. The methods were able to identify the correct source directions in nearly all image realizations.

To directly compare the various algorithms, we evaluated the performance of each method as a function of the number of detected source sequences for a fixed number (1000) of detected background sequences. Again, no energy or position filters were applied to the data. Using a simulated ^{137}Cs source again located at 22.5˚, we calculated the percentage of image realizations in which the source was correctly identified. To be considered correct, the algorithms must point within ±15˚ of the true source position.

TABLE I. PERCENTAGE OF CORRECT DIRECTION DETERMINATIONS (1000 DETECTED BACKGROUND SEQUENCES)

# Source Sequences	Sum (%)	Max (%)	Stat (%)	Clus (%)	Dens (%)
25	46	11	0	20	9
50	51	29	4	51	35
75	80	69	34	91	67
100	88	84	65	98	90
200	99	98	100	100	99

The number of detected source sequences was varied from 25 to 200 resulting in a background-to-source detected sequences ratio ranging from 40:1 to 5:1. At 662 keV, the number of imaged sequences is approximately 20% of the number of detected sequences (lost sequences are due to single events, kinematically infeasible Compton sequences, and mismatched energies), while for the background, only ~10% are imaged. Thus the imaged sequence ratios range from approximately 20:1 to 2.5:1. The results of these calculations are shown in Table I.

The summation and cluster methods outperformed the others at all levels of source activity. The statistical method performed poorly for low source counts, which is not surprising; the benefit of this method is primarily in discrimination between sources and background. As can be seen in Figs. 1 – 3, the statistical method rarely points in the wrong direction; it simply does not produce an answer when none can be determined.

The summation method is simple to implement and is capable of locating up to five or six well separated sources around the detector. The cluster method, which performed as well as or better than summation at all but the lowest number of detected source sequences, could potentially identify more sources, because the information is not collapsed into the heading dimension until after the clusters are identified. Additionally, the cluster method enables energy-dependent direction determination because the energy information is not discarded. For example, the cluster method could potentially identify a ^{137}Cs source in one direction and a ^{133}Ba source in the opposite direction. With addition of isotope identification analysis into the directionality algorithms, such determinations may be possible in GammaTracker.

IV. IMPLEMENTATION

The GammaTracker instrument uses a field programmable gate array (FPGA) to process raw data from the detector array. Ideally, the directionality algorithm would be implemented on this device to allow the main single-board computer to focus on the user interface. Thus, accuracy, simplicity, execution speed, and required memory are key issues in determining which algorithm(s) to incorporate into the instrument.

The speed at which each algorithm runs depends highly on the implementation of the method, the number of cones imaged, and (for two of the methods) the number of pixels in the image. Memory usage also depends on the implementation of the algorithms. The image generation step required for the maximization method—arguably the largest amount of memory needed for any single calculation—requires approximately 16 kB of storage, which is fairly modest for the on-board FPGA. The low-resolution directionality calculations in the GammaTracker instrument contrasts to other systems that display high-resolution gamma-ray images to the user. However, the key objective is to indicate which way the user must walk to find the source, so lower-resolution calculations are possible.

Based on the limited testing described in Section III, the summation and cluster methods are the most accurate algorithms tested for the pointing capability needed in GammaTracker. The clustering method does not rely on the generation of a 4π spherical image, making it a potentially better option for GammaTracker. One could further reduce the complexity of the cluster method by restricting the computations to lattice points on the unit sphere. Discretizing the intersection points in this manner would allow the instrument to only perform one set of calculations if several intersection points fell close together.

Additional testing is required to determine, for example, how well each algorithm responds to background-only source distributions and to estimate processing speeds on the FPGA. Moreover, incorporating isotope identification directly into the cluster algorithm may enable isotopic directionality capability. Finally, it may be beneficial to implement more than one algorithm in parallel and compare results to confirm the presence and direction of a source.

REFERENCES

[1] C. E. Seifert, M. J. Myjak, D. V. Jordan, "Simulated performance of the Gamma Tracker CdZnTe handheld radioisotope identifier," *IEEE Nucl. Sci. Symp. Conf. Record*, vol. 2, pp. 940-944, 2007.

[2] M. J. Myjak, S. J. Morris, R. W. Slaugh, J. M. McCann, L. J. Kirihara, J. S. Rohrer, B. J. Burghard, C. E. Seifert, "Electronics system for the GammaTracker handheld CdZnTe detector," *IEEE Nucl. Sci. Symp. Conf. Record*, vol. 1, pp. 509-510, 2007.

[3] F. Zhang, Z. He, D. Xu, G. F. Knoll, D. K. Wehe, and J. E. Berry, "Improved resolution for 3-D position-sensitive CdZnTe spectrometers," *IEEE Trans. Nucl. Sci.*, vol. 51, no. 5, pp. 2427–2431, Oct. 2004.

[4] M. J. Myjak, C. E. Seifert, "Real-time Compton imaging for the GammaTracker handheld CdZnTe detector," IEEE Trans. Nucl. Sci., vol. 55, no. 2, pp. 769-777, 2008.

[5] A. W. Lackie, K. L. Matthews II, B. M. Smith, W. Hill, W.-H. Wang, and M. L. Cherry, "A directional algorithm for an electronically-collimated gamma-ray detector," submitted to *IEEE Nucl. Sci. Symp.Conference. Record*, San Diego, CA, Oct. 2006.

[6] W. R. Kaye, N. D. Bennett, C. G. Wahl, Z. He, W. Wang, "Gamma-ray source location by attenuation measurements," *IEEE Nucl. Sci. Symp. Conf. Record*, vol. 2, pp. 1294-1298, 2007.

[7] S. Agostinelli et al, "G4—a simulation toolkit," *Nucl. Instr. Meth. Phys. Res.*, vol. A506, no. 3, pp. 250–303, Jul. 2003.